Designer topological insulator with enhanced gap and suppressed bulk conduction in Bi_2Se_3/Sb_2Te_3 ultra-short period superlattices

Ido Levy[1,2], Cody Youmans[3,4], Thor Axtmann Garcia[1,2], Haiming Deng[3,4], Steven Alsheimer[3], Christophe Testelin[5], Lia Krusin-Elbaum[3,4], Pouyan Ghaemi[3,4], Maria C. Tamargo[1,2,4]

[1] Department of Chemistry, The City College of New York, New York, NY 10031
[2] Chemistry Program, Graduate Center of CUNY, New York, NY 10021
[3] Department of Physics, The City College of New York, New York, NY 10031
[4] Physics Program, Graduate Center of CUNY, New York, NY 10021
[5] Sorbonne Université, CNRS, Institut des NanoSciences de Paris, 4 Place Jussieu, F-75005 Paris, France

Abstract

A novel approach to suppress bulk conductance in 3D topological insulators (TIs) using short period superlattices (SL) of two TIs is presented. Evidence for superlattice gap enhancement (SGE) was obtained from the reduction of bulk background doping from $1.2x10^{20}cm^{-3}$ to $8.5x10^{18}cm^{-3}$ as the period of Bi_2Se_3/Sb_2Te_3 SLs is decreased from 12nm to 5nm. Tight binding calculations show that in the ultra-short period regime, a significant SGE can be achieved for the resulting SL. Ultra-thin short period SLs behave as new designer TIs with bulk bandgaps up to 60% larger than the bandgap of the constituent layer of largest bandgap, while retaining topological surface features. Evidence for gap formation was obtained from ellipsometric measurements. Analysis of the weak anti-localization cusp in low temperature magneto-conductance confirms that the top and bottom surfaces of the SL structure behave as Dirac surfaces. This approach represents a promising platform for building truly insulating TIs.

Keywords: topological insulator, molecular beam epitaxy, superlattice, gap enhancement, Bi_2Se_3, Sb_2Te_3

There is currently much excitement around the novel physics and potential device applications of 3D topological insulators (TIs) [1-3]. A bandgap in the bulk, which renders them bulk insulators, along with metallic helical surface states are the principal properties that garner interest in their research. The TI's surface provides a novel electronic state that would harvest exotic quasi-particles, such as Majorana fermions, and other phenomena [4-6]. Groundbreaking potential applications such as quantum computing are envisioned [7]. The most widely studied of these materials is Bi_2Se_3 due to its relatively large bandgap and single surface Dirac cone, but other group V-chalcogenides such as Bi_2Te_3 and Sb_2Te_3 are also of great interest [8].

Despite their attractive properties, the relatively small bandgap of these materials of a few hundred meV, and the ease of formation of electrically active defects[9] result in high bulk conductivities, masking the features of their exotic surface states. In particular, when grown by molecular beam epitaxy (MBE), bulk Bi_2Se_3 is n-type[10] and Sb_2Te_3 is p-type [11]. Many attempts to reduce the bulk carrier density in TIs have been reported, including modification of the growth conditions and the substrates used [11, 12], impurity compensation doping [13-15], and the growth of mixed alloys [16]. Despite observed reduction of bulk conductivity through these methods, it is evident that significant improvement toward truly insulating bulk TIs needs the invention of fundamentally new protocols.

Band structure engineering by superlattice (SL) formation has been widely applied to semiconductor physics and devices [17, 18] for decades. In the field of topological materials, attempts to combine TI layers with trivial semiconductors or combining two topologically trivial materials to get 3D TIs has been explored. Recently, SLs of Bi_2Se_3/In_2Se_3 [19-21] have shown that the bandgap and the Dirac cone of the Bi_2Se_3 could be modified by the SL structure. Another system, ZnCdSe/Bi_2Se_3 SLs, showed multiple topological surface channels that scale with the number of SL periods [22]. A few examples of the growth and properties of heterojunctions and SLs comprised of two TI materials, such as Bi_2Te_3/Sb_2Te_3, have also been previously reported [23-26], however the effect of short period TI/TI SLs on the band structure and carrier density of the resulting materials, or on their topological surface states, has not been appreciably addressed.

In this work we report the growth of short-period SLs of alternating Bi_2Se_3 and Sb_2Te_3, (TI/TI SLs) which have a type-III or "broken gap" band alignment. In type-III band alignment both the valence and the conduction band extrema of one of the constituent materials lie above or below those of the other one, and the bandgaps of the two materials do not overlap[27]. The TI SL structures show a reduction of the bulk carrier density and an increase of the bulk resistivity as a function of the SL period thickness, while still retaining the topological surface states. We interpret this as evidence of new bulk bandgap formation in the SL material that increases with reduced period thickness. Tight binding calculations confirm that for certain materials parameters and TI/TI SL period, new "designer" 3D TI phases can be achieved with bulk bandgaps significantly larger than the bandgaps of either of the constituent layers. This novel approach to materials design and band structure engineering offers much promise for the realization of new TI materials with wider bandgaps than those available in bulk TIs and represents a promising and novel platform for building truly insulating bulk topological materials.

A series of SL samples consisting of alternating thin layers of Bi_2Se_3 and Sb_2Te_3 were grown by MBE and their structural properties were investigated by high resolution X-ray diffraction (HRXRD) and transmission electron microscopy (TEM). The SL structures were grown on a Bi_2Se_3 buffer layer on (0001) c-plane sapphire substrates with a 0.2° off-cut. A Riber 2300P MBE system was used with background pressures of 3-5x10^{-10} torr during growth. Samples with different SL period thicknesses, as well as different ratios of individual Bi_2Se_3 to Sb_2Te_3 layer thickness were grown. All samples consist of seven periods of the two alternating materials. The samples were grown using our previously reported MBE growth procedure that ensures very smooth and nearly twin free single layer crystals [28]. Details of the growth are presented in the ***Supporting Information Section***.

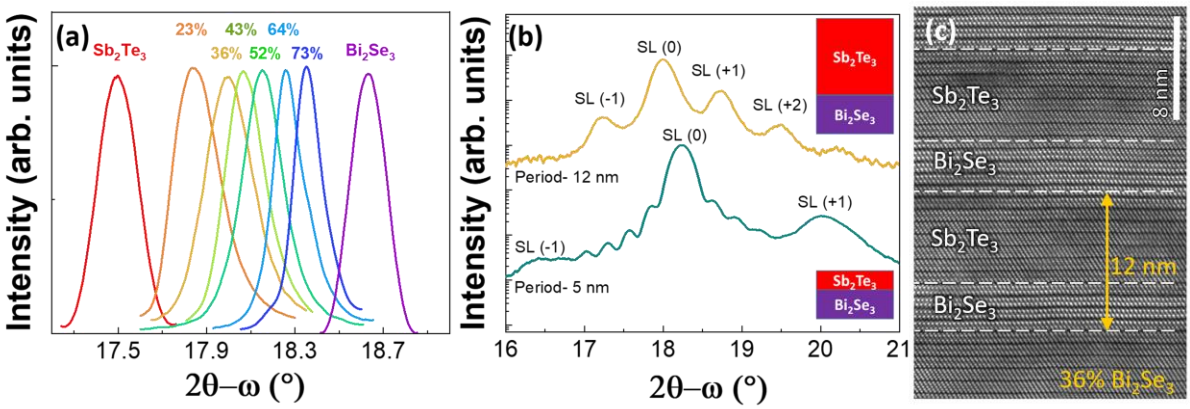

Figure 1: (a) HRXRD measurements of the (006) zero-order SL peaks, SL(0), of several of the SL samples studied and of pure Bi_2Se_3 and Sb_2Te_3. The peak position varied between that of the two pure materials providing a measure of the average composition of the SL. The colors of the spectra transitioning from purple to red, illustrate the gradual change in effective composition from pure Bi_2Se_3 to pure Sb_2Te_3. (b) Full HRXRD spectra of the (006) plane of the sample with 36% Bi_2Se_3 effective composition (top) and 52% effective composition (bottom). From the position of the SL satellite peaks [SL(+1), SL(-1) SL(+2)] the period of the SL could be calculated. **Insets:** period thicknesses with proportional layer thicknesses calculated from XRD. (c) HR-TEM cross-section image of the sample with 36% Bi_2Se_3 effective composition showing the alternating materials.

Scans of the HRXRD (006) reflection of the zero-order SL peak (Figure 1a), and the superlattice satellite peaks (Figure 1b) allowed us to calculate the effective composition of each sample, the thickness of the SL period [29], and the individual thicknesses of the Bi_2Se_3 and Sb_2Te_3 layers. The HRXRD measurements were performed using a Bruker D8 Discover diffractometer with a da-Vinci configuration and a Cu $K\alpha_1$(1.5418 Å) source to establish their crystal quality.

The good structural quality was also confirmed by the high resolution TEM (HR-TEM) image of the sample with 36% Bi_2Se_3 effective composition, which consisted of 4 nm Bi_2Se_3 and 8 nm Sb_2Te_3, as deduced from the HRXRD data. TEM measurements were performed (EAG Laboratories) using a Hitachi HD-2700 Spherical Aberration-Corrected Scanning-TEM with

Energy Dispersive X-ray Spectroscopy (EDS). The TEM image (Figure 1c) shows alternating layers with different contrast indicating the two different materials: the lighter contrast corresponding to the Bi_2Se_3 layer and the darker one to the Sb_2Te_3 layer. The calculated TEM thickness values agree well with the layer thicknesses extracted from the HRXRD measurements. In addition, the HR-TEM image clearly displays the quintuple layer (QL) structure of the individual layers, as well as the high crystallinity of the structure. Although atomically well ordered, the interfaces show some interface steps, or interface roughness, which appears more pronounced on the surfaces of the Sb_2Te_3 layers, consistent with observations that MBE grown Sb_2Te_3 has a higher degree of roughness than Bi_2Se_3 [11, 30].

Transport of all the samples was investigated by Hall Effect measurements, at 10K, using the van-der Pauw[31] (vdP) configuration with Indium contacts on a Lakeshore 7600 electromagnet system. The plot of the Hall resistance (R_{xy}) as a function of magnetic field (B) was used to learn the sample conductivity type (n- or p-type). All the samples were measured. Several representative plots are shown in Figure 2a. The corresponding effective composition for each sample is given in the figure. The sign of the slope dictates the conductivity type. We observed a transition of the SL conductivity from n-type to p-type at approximately 42% Bi_2Se_3 effective composition.

Carrier density for all the samples was also obtained from the Hall measurements at 10K. The bulk carrier density (carriers per cm^3) is plotted to correct for variations in total SL thickness among the samples. The data is plotted as a function of the $\%Bi_2Se_3$ effective composition in Figure 2b. In this analysis, it was anticipated that the carrier density would reach a minimum at the transition region between n-type to p-type behavior, as charge neutrality was achieved. This transition region is indicated in the figure by the bright region in the background separating the p-type samples from the n-type samples. However, no reduction in the carrier density near the transition region was evident in the data, suggesting that other factors are affecting the variations in conductivity of the samples. In fact, no correlation of carrier density with $\%Bi_2Se_3$ effective composition was evident in either the n-type (squares) or the p-type (circles) samples.

By contrast, a strong correlation is noted in Figure 2c, where the carrier density is plotted as a function of the SL period. Although most of the samples studied are n-type (only five p-type samples were grown), both carrier types display a similar relationship. A reduced carrier density for the samples with smaller SL periods is clearly observed. More than an order of magnitude reduction in carrier density was obtained between the samples with larger periods (~12 nm) and those with smaller periods (~5 nm). The two data points for samples with period above 14 nm do not to follow this trend, and have been excluded from our discussion, since at sufficiently large layer thickness a superlattice behavior may no longer apply. The low carrier densities of our smaller period TI/TI SLs are comparable to the best values reported for the constituent TI materials grown by MBE directly on sapphire substrates [11, 12, 32, 33]. We believe that these values

can be significantly improved, as these results were achieved only by our first efforts. We propose that mastering the properties of TI/TI SLs provides a promising and yet to be explored platform for building truly insulating topological materials.

These observations can be understood based on simple band structure considerations. The heterostructure band alignments between Bi_2Se_3 and Sb_2Te_3 are illustrated in the insets of figure 2c. As previously noted, these two materials have a type-III, or "broken gap" band alignment, [34,35] and the MBE grown Sb_2Te_3 is p-type, while the Bi_2Se_3 is n-type. [9] As portrayed in the insets, the generation of a SL with small enough periodicity, modifies the band structure and produces new gaps that can be tuned by changing the SL period and thickness[36].

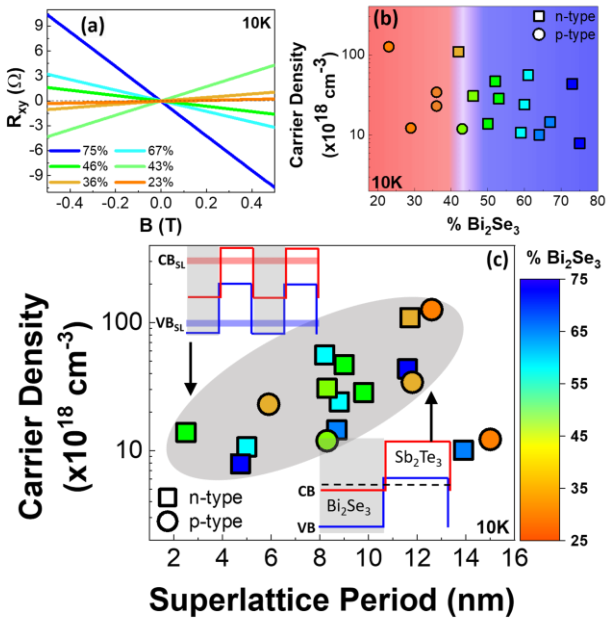

Figure 2: (a) Hall resistance plots of the SL samples. The effective composition is listed in the legend and illustrated by the color of the lines, as assigned in Figure 1a. (b) Carrier concentration of the samples as a function of the %Bi_2Se_3 effective composition. The bright vertical region indicates the composition at which the SL behavior changes from p-type (red background) to n-type (blue background). (c) Carrier concentration of the samples as a function of the SL period thickness, (shaded region is drawn to aid the eye). The color of the symbols in (b) and (c) corresponds to the effective compositions, as indicated in the bar of part (c). Insets illustrate the type III band alignment between Bi_2Se_3 and Sb_2Te_3 and band diagram of the SL. The small period SL results in the formation of a SL gap, which can be tuned by the period and layer thicknesses.

A better understanding of the properties of these short period TI/TI SLs, and the possibilities of band structure engineering in these novel materials can be obtained from tight binding calculations. Since the alternating layers consist of only a few single layers of each material, we are effectively developing a new type of material and tight binding is the appropriate method to derive the band structure of our new compound.

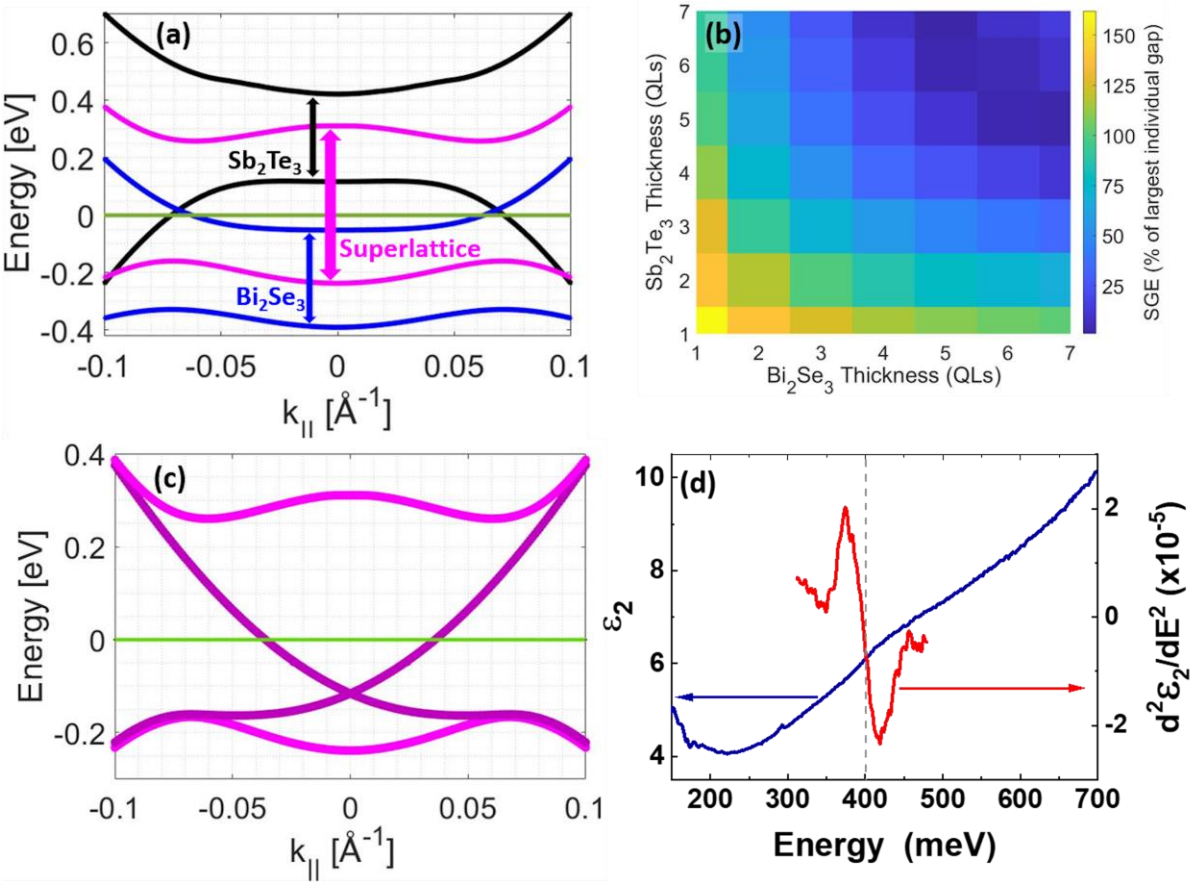

Figure 3: (a) Bulk band gaps of Bi_2Se_3 (blue), Sb_2Te_3 (black), and of an ultrathin binary SL (magenta) of Bi_2Se_3 and Sb_2Te_3 with respective layer thicknesses n(Bi_2Se_3)=1 QL and n(Sb_2Te_3)=1 QL. (b) SGE dependence on short-period SL layer thicknesses. (c) Bulk gap and subgap edge-bands of the SL considered in part (a). (d) Imaginary component of the dielectric constant ε_2, obtained from ellipsometric measurements at room temperature, and its second derivative $\frac{d\varepsilon_2}{dE^2}$, for a SL with a period of 5QL. A dashed line indicates the optical onset E_{opt}, clearly identified by the inflection point of the second derivative curve.

The low energy properties of both Bi_2Se_3 and Sb_2Te_3 are well described by the effective k.p Hamiltonian introduced by Zhang et al. [37] Using the parameters from Ref. 38 we built a tight-binding model Hamiltonian. Figure 3(a) shows the resulting highest valence and lowest conduction bands for a SL with layer thicknesses n(Bi_2Se_3)=1 QL and n(Sb_2Te_3)=2 QL, compared with those of pure Bi_2Se_3 and Sb_2Te_3. The figure highlights an instance of the large superlattice gap enhancement (SGE) expected from the experiments detailed above. A bulk SL bandgap as high as ~160% of the Bi_2Se_3 bandgap is predicted in Figure 3(b) for the thinnest SL periods, supporting the proposal of significantly increased bandgaps with decreasing period thickness. We would like to stress that the material described by the calculation, consisting of a few QL of Sb_2Te_3 and a few QLs of Bi_2Se_3 can no longer be considered as alternating layers of the two bulk materials, as our simple diagrams of figure 2c suggest (as k.p calculations would do), but rather a new "designer" 3D material. Figure 3(c) demonstrates the preserved topological nature of the composite material by displaying the edge bands at a particular termination of the

SL (Bi_2Se_3 in our case), within the corresponding bulk band gap. Furthermore, in contrast with the two constituent materials the Fermi level in the resulting SL sample lies mid-gap and near the Dirac point, as desired for achieving truly insulating TIs. Thus, the new designer material formed by alternating thin layers of two constituent TIs is itself a new 3D TI with preserved topological surface states at the top and bottom surfaces of the SL, whose bulk bandgap increases as the period of the superlattice layers decreases. Details of the tight binding methodology is in the ***Supporting Information Section***.

To confirm the formation of a new bulk bandgap and subsequent gap enhancement, we have performed ellipsometric measurements on different SLs and on a reference Sb_2Te_3 layer, an approach recently used to study Bi_2Se_3 gap energy [39,40] (the experimental procedure is described in the ***Supporting Information Section).*** Figure 3(d) shows the imaginary component of the dielectric function (related to absorption) versus photon energy, measured for a 5QL period SL (2 Sb_2Te_3 QL- 3 Bi_2Se_3 QL). This curve is very similar to what was measured on $Bi_2Se_{3-x}Te_x$ epitaxial layers [39]. An onset, well determined by plotting the second derivative $\frac{d^2\varepsilon_2}{dE^2}$, is observed at an energy E_{opt} = 403 ± 10 meV. From this optical transition and the SL n-doping, it is possible to estimate the SL gap in the range $E_{gap} = 236 \pm 36\, meV$. This gap energy can be compared with that of Sb_2Te_3, 232 meV, also measured by ellipsometry, leading to a SGE 102 ± 16 %, very close to the predicted value of 105 % [fig. 3(b)]. By contrast, similar measurements on a sample with a period of 8QL showed no evidence of a transition within the explored energy range, consistent with a gap of ~70 meV or less, also predicted by the model. (***Supporting Information Section Figure S3***).

In order to investigate experimentally the presence of the topologically non trivial surface states in these new "designer" TI/TI SLs, as predicted by the tight binding calculations, magneto-conductance (M-C) measurements were performed at 2K on the sample with period of 5nm. The M-C measurements were performed in a 14 Tesla Quantum Design Physical property measurement system (PPMS) in 1 mTorr (at low temperature) of He gas. Electrical contacts in the vdP configuration were made with indium bonded on the edge of the thin film. The M-C measurements, shown in Figure 4a, exhibit a weak anti-localization (WAL) cusp, the trademark of 2D transport channels [41,42]. The plot of the Hall resistance for the same sample is also shown displaying a highly linear behavior consistent with single carrier behavior [43]. Additional details can be found in the ***Supporting Information Section***.

Further analysis of the data was carried out by fitting to the Hikami-Larkin-Nagaoka (HLN) 2D localization theory [44]. From this fit, we extracted a value to the fitting parameter α of 1.0 for the small period (5nm) sample. It has been shown that the parameter α is proportional to the number of 2D channels in the layer, where α= 0.5 represents one channel. Our results suggest that the SL sample behaves like a new 3D TI material with only the top and bottom surfaces of the structure hosting topological surface states.

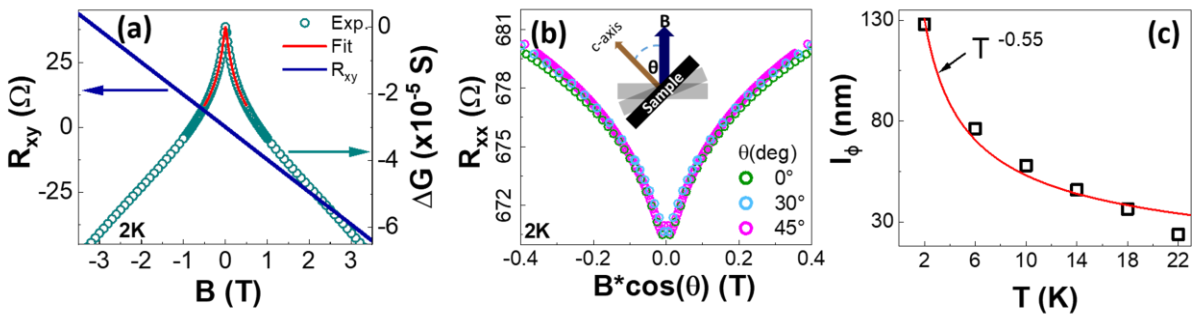

Figure 4: (a) Magneto-conductance of the sample with 5nm SL period thickness showing a weak anti-localization (WAL) cusp. A fit to the HLN theory, shown in red, gives a value of $\alpha = 1$. Hall resistance for the sample is also shown as a function of the magnetic field (B). (b) Angle dependent magnetoresistance of the 5nm period SL as a function of the transverse component of magnetic field, $B\perp=B*\cos(\theta)$. (c) Temperature dependence of dephasing length l_φ for the same sample as in parts a and b.

Angle dependent magneto-resistance for the same sample are presented in Figure 4b, where the magneto-resistance, measured with the magnetic field at different angles (θ) normal to the sample surface, is plotted as a function of the transverse component of the magnetic field. All the plots collapse to one curve, suggesting that the 2D conductance channels resulted from the surface electrons. Finally, the M-C as a function of temperature was also measured. The dephasing length (l_φ) plotted as a function of temperature is shown in Figure 4c. The data fits well to a temperature dependence of $T^{-0.55}$, very close to the ideal $T^{-0.5}$ dependence predicted by HLN theory for 2D conduction channels[45]. This reinforces our conclusion that the SL sample behaves as a new "designer" 3D TI phase with a bandgap in the bulk and topological surface states at the top and bottom surfaces of the sample. Furthermore, the residual bulk conductivity of the new "designer" TI material can be adjusted by the appropriate choice of SL parameters due to a large SGE possible for ultra-thin period SLs.

This work presents a novel approach to band structure engineering and reduced background doping of topological insulators by the use of ultra-thin period TI/TI SLs. An observed reduction of bulk background doping by more than one order of magnitude as the period of the SLs decreases from 12 nm to 5 nm can be understood on the basis of a SGE possible in type-III "broken gap" heterostructures. This interpretation is supported by tight binding calculations, and experimentally confirmed by optical ellipsometry. We show, from M-C measurements, that the topological surface states of the grown TI/TI SL with the 5QL period are in fact preserved. Thus, a new "designer" 3D topological insulator material with enhanced bulk bandgap and preserved helical surface states is produced. This approach represents a promising and yet to be explored novel platform for building truly insulating bulk topological materials.

Acknowledgements:

This work was supported by NSF Grant Nos. DMR-1420634 (MRSEC PAS[3]), HRD-1547830 (IDEALS CREST) and DMR-1824265.

Author Contributions:

I.L, T.A.G. and M.C.T. conceived the experiment and executed the crystal growth. I.L. performed HR-XRD and XRR measurements. S.A. and I.L. performed and analyzed the 10K Hall Effect measurements. H.D. and L.K.E performed the 2K magneto conductance measurements. C.Y. and P.G. carried out the analytical theoretical modeling. C.T. and I.L. performed and analyzed the optical measurements. I.L., C.Y., P.G., C.T. and M.C.T. wrote and reviewed the manuscript. All authors contributed to interpretation of the data and discussions.

Competing Interests: The authors declare no competing interests

Corresponding Author: Maria C. Tamargo (mtamargo@ccny.cuny.edu)

Supporting Information:

The Supporting Information Section contains additional information and figures related to the A) growth and structural characterization, B) transport measurements, C) optical measurements, and D) theoretical modeling.

This material is available free of charge via the internet at https://urldefense.proofpoint.com/v2/url?u=http-3A__pubs.acs.org&d=DwIFaQ&c=4NmamNZG3KTnUCoC6InoLJ6KV1tbVKrkZXHRwtIMGmo&r=ITMH3RjXbkpRX6vih50v24G0u6c5RKaHpoAU8msQqPw&m=Sur3aZTukaCwZ80ZgFhnEU44jWJTQIwc5t48sTgO3ng&s=1KL_YGc7s2mC7nNtyy5dCcSzsitAdQRYiXaT008JUV4&e= .

References:

1. Qi, X. L.; Zhang, S. C. The quantum spin Hall effect and topological insulators. *Phys. Today* **2010,** 63**,** 33−38.
2. Hasan, M. Z.; Kane, C. L. Colloquium: Topological insulators. *Rev. Mod. Phys.* **2010,** 82, 3045−3067.
3. Qi, X. L.; Zhang, S. C. Topological insulators and superconductors. *Rev. Mod. Phys.* **2011,** 83, 1057−1110.
4. Fu, L.; Kane, C. L. Superconducting proximity effect and Majorana fermions at the surface of a topological insulator. *Phys. Rev. Lett.* **2008,** 100, 096407.
5. Stanescu, T. D.; Sau, J. D.; Lutchyn, R. M.; Das Sarma, S. Proximity effect at the superconductor-topological insulator interface. *Phys. Rev. B* **2010,** 81, 241310.
6. Read, N. Topological phases and quasiparticle braiding. *Phys. Today*, **2012,** 65, 38−43.
7. Moore, J. E. The birth of topological insulators. *Nature* **2010,** 464, 194−198.
8. Zhang, H.; Liu, C. X.; Qi, X. L.; Dai, X.; Fang Z.; Zhang, S. C. Topological insulators in Bi_2Se_3, Bi_2Te_3 and Sb_2Te_3 with a single Dirac cone on the surface. *Nat. Phys.* **2009,** 5, 438–442.
9. West, D.; Sun, Y. Y.; Wang, H.; Bang, J.; Zhang, S. B. Native defects in second-generation topological insulators: Effect of spin-orbit interaction on Bi_2Se_3. *Phys. Rev. B* **2012,** 86, 121201.
10. He, L.; Xiu, F.; Wang, Y.; Fedorov, A. V.; Huang, G.; Kou, X.; Lang, M.; Beyermann, W. P.; Zou, J.; Wang, K. L. Epitaxial growth of Bi_2Se_3 topological insulator thin films on Si (111). *J. Appl. Phys* **2011,** 109, 103702.
11. Thiet, D. V.; Quang, V. N.; Hai, N. T. M.; Huong, N. T.; Cho, S.; Tuan, D. A.; Dung, D. D.; Tam, T. V. Optimizing the carrier density and thermoelectric properties of Sb_2Te_3 films by using the growth temperature. *J. Korean Phys. Soc.* **2018,** 72, 915–919.
12. Koirala, N.; Brahlek, M.; Salehi, M.; Wu, L.; Dai, J.; Waugh, J.; Nummy, T.; Han, M. G.; Moon, J.; Zhu, Y.; Dessau, D.; Wu, W.; Armitage, N. P.; Oh, S. Record surface state mobility and quantum Hall effect in topological insulator thin films via interface engineering. *Nano Lett.* **2015,** 15, 8245–8249.
13. Hong, S. S.; Cha, J. J.; Kong, D.; Cui, Y. Ultra-low carrier concentration and surface-dominant transport in antimony-doped Bi_2Se_3 topological insulator nanoribbons. *Nat. Commun.* **2012,** 3, 757.
14. Chen, Y.; L. Analytis, J. G.; Chu, J. H.; Liu, Z. K.; Mo, S. K.; Qi, X. L.; Zhang, H. J.; Lu, D. H.; Dai, X.; Fang, Z.; Zhang, S. C.; Fisher, I. R.; Hussain, Z.; Shen Z. X. Experimental realization of a three-dimensional topological insulator, Bi_3Te_2. *Science* **2009,** 325, 178–181.
15. Ginley, T. P.; Wang, Y.; Law, S. Topological insulator film growth by molecular beam epitaxy: A review. *Crystals* **2016,** 6, 154.

16. Bao, L.; He, L.; Meyer, N.; Kou, X.; Zhang, P.; Chen, Z. G.; Fedorov, A. V.; Zou, J.; Riedemann, T. M.; Lograsso, T. A.; Wang, K. L.; Tuttle, G.; Xiu, F. Weak antilocalization and quantum oscillations of surface states in topological insulator Bi_2Se_2Te. *Sci. Rep.* **2012,** 2, 726.

17. Esaki, L.; Chang, L. L. New transport phenomenon in a semiconductor "superlattice". *Phys. Rev. Lett.* **1974,** 33, 495−498.

18. Fox, M.; Ispasoiu, R. Quantum wells, superlattices, and band-gap engineering. In: Kasap, S.; Capper, P. (eds) Springer handbook of electronic and photonic materials. Springer Handbooks. Springer, Cham **2017.**

19. Belopolski, I.; Xu, S. Y.; Koirala, N.; Liu, C.; Bian, G.; Strocov, V. N.; Chang, G.; Neupane, M.; Alidoust, N.; Sanchez, D.; Zheng, H.; Brahlek, M.; Rogalev, V.; Kim, T.; Plumb, N. C.; Chen, C., Bertran, F., Le Fèvre, P., Taleb-Ibrahimi, A., Asensio, M. C., Shi, M.; Lin, H.; Hoesch, M.; Oh, S.; Hasan, M. Z. A novel artificial condensed matter lattice and a new platform for one-dimensional topological phases. *Sci. Adv.* **2017,** 3, e1501692.

20. Wang, Z. Y.; Guo, X.; Li, H. D.; Wong, T. L.; Wang, N.; Xie, M. H. Superlattices of Bi_2Se_3/In_2Se_3: Growth characteristics and structural properties. *Appl. Phys. Lett.* **2011,** 99, 023112.

21. Zhao, Y.; Liu H.; Guo, X.; Jiang, Y.; Sun, Y.; Wang, H.; Wang, Y.; Li, H. D.; Xie, M. H.; Xie X. C.; Wang, J. Crossover from 3D to 2D quantum transport in Bi_2Se_3/In_2Se_3 superlattices. *Nano Lett.* **2014,** 14, 5244−5249.

22. Chen, Z.; Zhao, L.; Park, K.; Garcia, T. A.; Tamargo, M. C.; Krusin-Elbaum, L. Robust topological interfaces and charge transfer in epitaxial Bi_2Se_3/II−VI semiconductor superlattices. *Nano Lett.* **2015,** 15, 6365–6370.

23. Narendra, N.; Kim, K. W. Toward enhanced thermoelectric effects in Bi_2Te_3/Sb_2Te_3 heterostructures. *Semicond. Sci. Technol.* **2017,** 32, 035005.

24. Touzelbaev, M. N.; Zhou, P.; Venkatasubramanian, R.; Goodson, K. E. Thermal characterization of Bi_2Te_3/Sb_2Te_3 superlattices. *J. Appl. Phys.* **2001,** 90, 763–767.

25. Hinsche, N. F.; Yavorsky, B. Y.; Gradhand, M.; Czerner, M.; Winkler, M.; Konig, J.; Bottner, H.; Mertig, I.; Zahn, P. Thermoelectric transport in Bi_2Te_3/Sb_2Te_3 superlattices. *Phys. Rev. B* **2012,** 86, 085323.

26. Lanius, M.; Kampmeier, J.; Weyrich, C.; Kölling, S.; Schall, M.; Schüffelgen, P.; Neumann, E.; Luysberg, M.; Mussler, G.; Koenraad, P. M.; Schäpers, T.; Grützmacher, D. P–N junctions in ultrathin topological insulator Sb_2Te_3/Bi_2Te_3 heterostructures grown by molecular beam epitaxy. *Cryst. Growth Des.* **2016,** 16, 2057−2061.

27. Plis, E. InAs/GaSb type-II superlattice detectors. *Adv. Electron.* **2014**, 246769, (2014)

28. Levy, I.; Garcia, T. A.; Shafique, S.; Tamargo, M. C. Reduced twinning and surface roughness of Bi_2Se_3 and Bi_2Te_3 layers grown by molecular beam epitaxy on sapphire substrates. *J. Vac. Sci. Technol. B* **2018,** 36, 02D107.

29. Vandenberg, J. M.; Hamm, R. A.; Macrander, A. T.; Panish, M. B.; Temkin, H. Structural characterization of GaInAs(P)/InP quantum well structures grown by gas source molecular beam epitaxy. *Appl. Phys. Lett.* **1986,** 48, 1153–1155.
30. Richardella, A.; Zhang, D. M.; Lee, J. S.; Koser, A.; Rench, D. W.; Yeats, A. L.; Buckley, B. B.; Awschalom, D. D.; Samarth, N. Coherent heteroepitaxy of Bi_2Se_3 on GaAs (111)B. *Appl. Phys. Lett.* **2010,** 97, 262104.
31. Van der Pauw, L. J. A method for measuring the resistivity and hall coefficient on lamellae of arbitrary shape. *Philips Tech. Rev.* **1958,** 20, 220–224.
32. Satake, Y.; Shiogai, J.; Takane, D.; Yamada, K.; Fujiwara, K.; Souma, S.; Sato, T.; Takahashi, T.; Tsukazaki, A. Fermi-level tuning of the Dirac surface state in $(Bi_{1-x}Sb_x)_2Se_3$ thin films. *J. Phys.: Condens. Matter* **2018,** 30, 085501.
33. Tabor, P.; Keenan, C.; Urazhdin, S.; Lederman, D. Molecular beam epitaxy and characterization of thin Bi_2Se_3 films on Al_2O_3 (110). *Appl. Phys. Lett.* **99**, 013111 (2011)
34. Takane, D.; Souma, S.; Sato, T.; Takahashi, T.; Segawa, K.; Ando Y. Work function of bulk-insulating topological insulator $Bi_{2-x}Sb_xTe_{3-y}Se_y$. *Appl. Phys. Lett.* **2016,** 109, 091601.
35. Menshchikova, T. V.; Ostrokov, M. M.; Tsirkin, S. S.; Samorokov, D. A.; Bebneva, V. V.; Ernst, A.; Kuznetsov, V. M.; Chulkov, E. V. Band structure engineering in topological insulator based heterostructures. *Nano Lett.* **2013,** 13, 6064–6069.
36. Zakharova, A.; Yen, S. T.; Chao, K. A. Strain-induced semimetal-semiconductor transition in InAs/GaSb broken-gap quantum wells. *Phys. Rev. B* **2012,** 66, 085312.
37. Liu, C. X.; Qi, X. L.; Zhang, H.; Dai, X.; Fang, Z.; Zhang, S. C. Model Hamiltonian for topological insulators. *Phys. Rev. B* **2010,** 82, 045122.
38. Nechaev, I. A.; Krasovskii, E. E. Relativistic k · p Hamiltonians for centrosymmetric topological insulators from ab initio wave functions. *Phys. Rev. B* **2016,** 94, 201410(R).
39. Dubrovka, A.; Caha, O.; Hroncek, M.; Fris, P.; Orlita, M.; Holy, V.; Steiner, H.; Bauer, G.; Springholz, G. and Humlicek, J. Interband absorption edge in the topological insulators Bi2(Te1−xSex)3, Phys. Rev. B **2017**, 96, 235202,
40. Post, K. W.; Chapler, B. C.; He, L.; Kou, X.; Wang, K. L. and Basov, D. N., Thickness-dependent bulk electronic properties in Bi2Se3 thin films revealed by infrared spectroscopy, Phys. Rev. B **2013**, 88, 075121,
41. Steinberg, H.; Laloe, J. B.; Fatemi, V.; Moodera, J. S.; Jarillo-Herrero P. Electrically tunable surface-to-bulk coherent coupling in topological insulator thin films, *Phys. Rev. B* **2011,** 84, 233101.
42. Chen, J.; He, X. Y.; Wu, K. H.; Ji, Z. Q.; Lu, L.; Shi, J. R.; Smet, J. H.; Li, Y. Q. Tunable surface conductivity in Bi_2Se_3 revealed in diffusive electron transport. *Phys. Rev. B* **2011** 83, 241304(R).
43. Eschbach, M.; Mlynczak, E.; Kellner, J.; Kampmeier, J.; Lanius, M.; Neumann, E.; Weyrich, C.; Gehlmann, M.; Gospodaric, P.; Doring, S. et al., Realization of a vertical

topological p-n junction in epitaxial Sb_2Te_3/Bi_2Te_3 heterostructure, Nat. Comm. **2015**, 6, 8816.

44. Hikami, S.; Larkin, A. I.; Nagaoka, Y. Spin-orbit interaction and magnetoresistance in the two dimensional random system. *Prog. Theor. Phys.* **1980,** 63, 707–710.

45. Altshuler, B. L.; Aronov, A. G.; Khmelnitsky, D. E. Effects of electron-electron collisions with small energy transfers on quantum localisation. *J. Phys. C: Solid State Phys.* **1982,** 15, 7367–7386.